European Council for Nuclear Research

Summer Student Report

Within the framework of the GBAR experiment

"Analysis of Positronium Anihilation Within the Reaction Chamber of the GBAR Project"

ATILIO ALBERTO RODRÍGUEZ MIRANDA
CERN ID: 183844

SUPERVISORS: PAULINE COMINI & LISZKAY LASLO

JULY, 2024

Contents

List of Figures

PART I

Summer Student Report

CHAPTER 1

Abstract

This project IS focused on the detailed analysis of positronium annihilation within the reaction chamber of the GBAR experiment at CERN (Gravitational Behavior of Antihydrogen at Rest). The study aimed to investigate positronium through single-shot measurements, providing insights into its annihilation processes with high precision.

Key Objectives and Methods:

- *Positronium Formation and Detection:* Positrons are introduced into the reaction chamber to form positronium. The annihilation events should be detected using lead tungstate (PWO) scintillators, known for their excellent energy resolution and high density, which were critical for accurate measurements.
- *Experimental Setup:* The detection system was analyzed for high-resolution measurements to capture precise annihilation events. The experiment was conducted under controlled conditions to ensure stability and reliability.
- *Data Analysis:* Detailed analysis of the annihilation events was performed to determine the energy characteristics and dynamics of the annihilation products.

Significance:

- *Cross-Section Determination:* Accurate measurement of positronium annihilation contributes to the precise determination of cross sections for antiprotons and antihydrogen (H and H-bar) generated in the reaction chamber. This data is crucial for validating theoretical predictions and improving our understanding of particle interactions.
- *Technological Advancement:* The use of PWO scintillators in this context enhances the capability to measure high-energy gamma rays with precision, advancing experimental techniques in particle physics.

This project significantly enhances our understanding of positronium annihilation and provides valuable data for the study of antiparticle interactions within the GBAR experiment.

CHAPTER 2

GBAR Experiment

2.1 Overview of the GBAR Experiment

Einstein's Weak Equivalence Principle states that the trajectory of a test particle, when subjected only to a gravitational force, is independent of the particle's composition and internal structure. This means that all particles, regardless of their internal properties, fall under the influence of gravity in the same way when only gravitational interaction is considered.

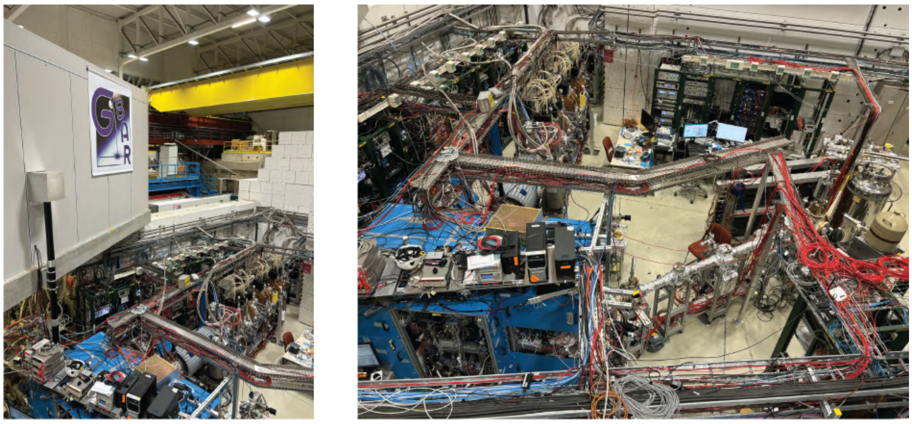

Figure 2.1: GBAR Facility inside the Antimatter Factory. In the image, the positron beamline and the shielding around the reaction chamber are visible.

The GBAR (Gravitational Behaviour of Antihydrogen at Rest) experiment aims to support this weak equivalence principle by measuring the modulus of the terrestrial gravitational acceleration of antihydrogen. By doing so, the experiment seeks to verify whether antihydrogen, composed of an antiproton and a positron, follows the same free-fall law in a gravitational field as normal hydrogen, thus confirming the universality of gravity.

The objectives of the Gravitational Behaviour of Antihydrogen at Rest (GBAR) project are as follows:

1. Production of Antihydrogen: To generate antihydrogen atoms, which are the antimatter counterparts of hydrogen atoms and consist of a positron and an antiproton.
2. Sympathetic Cooling: To achieve temperatures on the order of microkelvins (K) through sympathetic cooling techniques, which significantly reduce the kinetic energy of antihydrogen atoms.
3. Photodetachment of the Outter Positron: To perform the photodetachment of the external positron from the antihydrogen ion in order to precisely measure the gravitational acceleration of antihydrogen, which will allow for the assessment of its behavior under the influence of gravity.

The reactions for the obtention of antihydrogen and anti-ions, are shown on equations 2.1 and 2.2, respectively.

$$\bar{p} + \mathrm{Ps} \rightarrow \bar{H} + e^{-} \tag{2.1}$$

$$\bar{H} + \mathrm{Ps} \rightarrow \bar{H}^{+} + e^{-} \tag{2.2}$$

One further specific goal of the GBAR experiment is the measurement of the Lamb shift in antihydrogen. The Lamb shift refers to the observed deviation in the energy levels of hydrogen that cannot be explained by non-relativistic quantum mechanics alone. This effect was predicted by quantum field theory and observed experimentally in hydrogen atoms. Specifically, GBAR aims to measure the Lamb shift of the 2s state of antihydrogen. Such a measurement would be significant for testing CPT symmetry (Charge, Parity, Time) and verifying Lorentz invariance.

2.2 Componentes of the GBAR Experiment

The main components of the Gravitational Behaviour of Antihydrogen at Rest (GBAR) project are as follows:

1. Positron Beam and Positron Traps: A positron beam is directed towards a specific target. The system includes traps designed for the accumulation and storage of positrons, which are essential for antihydrogen production.
2. Antiproton Beam and Deceleration System: An antiproton beam is provided by ELENA (Extra Low ENergy Antiproton ring). This beam is decelerated using a pulsed drift tube decelerator and stored in an antiproton trap.
3. **Reaction Chamber**: *This is the main scenario for the development of my internship project.* In this chamber, positronium is produced from the positron beam. The positronium is excited with a laser within the chamber, which also features a switchyard for the deposition of antions, antihydrogen, and the recycling of antiprotons.

4. Vacuum Chamber with Paul Traps: This vacuum chamber contains two Paul traps, which are used for the manipulation and storage of charged particles in a controlled environment.

5. Micro-MEGAS Tracker Detector and Scintillator Bar TOF Array: The detection system includes a micro-MEGAS (Micro-Mesh Gaseous Structure) tracker detector for precise particle localization, as well as a TOF (Time-of-Flight) array composed of scintillator bars, which measures the time-of-flight of particles for identification and analysis.

2.3 GBAR Milestones

The steps required for the success of the GBAR experiment are as follows:

1. **Production of an intense and fast positron beam:** A beam of positrons with energy in the MeV range must be generated from a thin tungsten target. This step is crucial for obtaining a sufficient quantity of positrons for the subsequent experiments.

2. **Selection and suppression of electrons and Compton background:** Positrons must be selected, and electrons and Compton background must be suppressed through magnetic separation techniques. This ensures that the positron beam is as pure as possible.

3. **Moderation of positrons:** The selected positrons need to be moderated to reduce their energy to suitable levels for the next stage of the process.

4. **Accumulation of positrons:** The moderated positrons must be accumulated before being injected into a porous silica material. This accumulation is necessary to form a cloud of ortho-positrons, which is essential for the subsequent interactions.

5. **Excitation of the positronium target:** The positronium target must be excited to significantly increase the cross-section factor for interaction with antihydrogen ($\bar{H}^+$). This is crucial for improving the efficiency of antihydrogen formation.

6. **Interaction with low-energy antiprotons:** Finally, the ortho-positronium must be made to interact with a low-energy antiproton beam provided by ELENA. This interaction is necessary for the formation of antihydrogen and for carrying out the proposed experiments.

7. **Accumulation of anti-ions $\bar{H}^+$:** Accumulate anti-ions $\bar{H}^+$ for sympathetic cooling down to 10 µK. This step is critical for achieving the required low temperatures for precise measurements.

8. **Photodetachment at threshold of excess positrons and measurement of free fall:** Perform photodetachment of excess positrons at the threshold energy and measure the free fall of antihydrogen. This measurement is essential for determining the gravitational acceleration of antihydrogen.

2.4 Production of Fast Positrons

During the positron generation process, a wide range of kinetic energies is observed. After the creation of positrons, a moderation process is required to achieve effective trapping. Initially, there is a flux of fast positrons at $10^{12}\frac{e^+}{s}$ before the moderation stage. The cross-section for positron-electron pair production increases significantly above 1.2 MeV; however, the beam must remain below 10 MeV to ensure radiological safety. By increasing the temperature in the target of the linear accelerator (Linac), the low cross-section for positron production is compensated, as this results in an increase in beam current.

2.5 Positronium Formation

The positron-positronium converter and its surroundings are a key component of the GBAR experiment. This converter's function is to form a dense cloud of positronium from an intense pulse of positrons provided by a High Field Trap.

The positron-positronium converter requires access for the antiproton beam, two accesses for counter-propagating laser beams (which excite the positronium), as well as an output for the antihydrogen and the H^+ anti-ion.

Positronium is a bound state of a positron and an electron. In its ground state, the triplet form (**ortho-positronium**) has a vacuum lifetime of 142 ns, while the singlet state (para-positronium) has a vacuum lifetime of 125 ps, which is significantly shorter than the duration of antiproton ($\bar{p}$) pulses. Therefore, a dense cloud of ortho-positronium serves as the target for the antiproton beam.

Converter Material Requirements

The requirements for the positron-positronium conversion material are:

1. **High positron vacuum:** To ensure higher efficiency in ortho-positronium formation, a high-quality vacuum environment is required to minimize unwanted collisions and positronium losses.

2. **Low kinetic energy of positronium:** The positronium should have low kinetic energy to maintain a high effective density of positrons at the surface of the converter, thereby facilitating ortho-positronium formation.

3. **Stability of the vacuum condition along the beam line:** Stability of the vacuum along the beam line is crucial to avoid fluctuations that could impact conversion efficiency and experiment quality.

4. **Stability of conversion efficiency under laser illumination and irradiation:** The material should maintain high conversion efficiency even under conditions of laser illumination and irradiation, ensuring effective positronium formation.

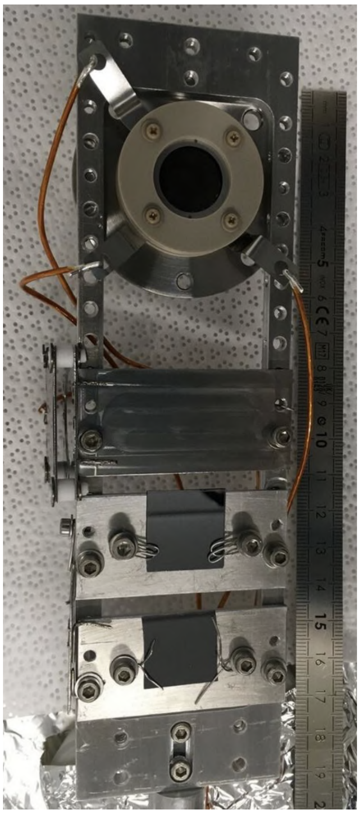

Figure 2.2: Moving target with silicon targets, mesoporous silica, and false target, along with MCP.

5. **Minimal need for in situ treatment:** Whenever possible, the material should require minimal in situ treatment, simplifying the operation and maintenance of the system.

The energy of the emitted positronium will depend on the *positron/positronium conversion material and the underlying physical process* [Kan+21], [Mil48] . The conversion material influences the efficiency of the positronium formation process and thus the energy of the emitted positrons. Specifically, the type of material and its properties affect the density and kinetic energy of the positrons, which directly impacts the characteristics of the generated positronium. Additionally, the underlying physical process, including the interaction between positrons and electrons, also plays a crucial role in determining the final energy of the positronium.

In materials where the positronium work function is negative, the energy of the emitted positronium will be relatively high. In most cases, positronium emission increases with temperature, especially when the kinetic energy of positronium exceeds 0.1 eV. This makes porous silica an excellent candidate for positron/positronium conversion.

Ortho-positronium emission is efficient in nanoporous silica films. Pure SiO_2 films exhibit porous structures with various sizes on the nanometer scale [BP80], with different degrees of interconnection. Positrons implanted in nanoporous silica films show varying depths of distribution, which follow the Makhovian implantation profile (2.3).

$$\bar{z} = AE^{1.6} \tag{2.3}$$

Where:

- E: Is the energy in KeV
- $A \approx \frac{400}{\rho} \frac{\text{Å}}{KeV1.6}$ (ρ is the density in g/cm^3)

By time of flight measurements it has been determined that the escaping energy of the positronioum, out of the porous silica, is 50 meV or less.

2.6 Antiprotons Beam Requirement

One of the main components for the production of antihydrogen is antiprotons ($\bar{p}$). The cross-section for antihydrogen production exhibits a peak at $\sigma_h \approx 1 \times 10^{-15}\,\text{cm}^2$ for an incident antiproton beam with a kinetic energy range of 0.5-15 keV. Due to the limited lifetime of positrons in the $n = 1$ state, the beam must be delivered in bunches of 100 ns. Additionally, the antiproton beam must spatially overlap with the positronium cloud to maximize the efficiency of antihydrogen production.

CHAPTER 3

Characterization of the PWO Detectors

3.1 PWO Detectors

In the experimental area of GBAR, four PWO detectors were available. These detectors were composed of two main components: a scintillator and a photomultiplier tube (PMT). The scintillator was made of lead tungstate, while the photomultiplier tube was a Hamamatsu brand. After performing the characterizations, the methodology of which is detailed in the following sections, we identified a defect in the PWO13 detector, which is specified at the end of this chapter. Functional detectors (PWO 12, PWO 14 & PWO 15) are presented in picture 3.1

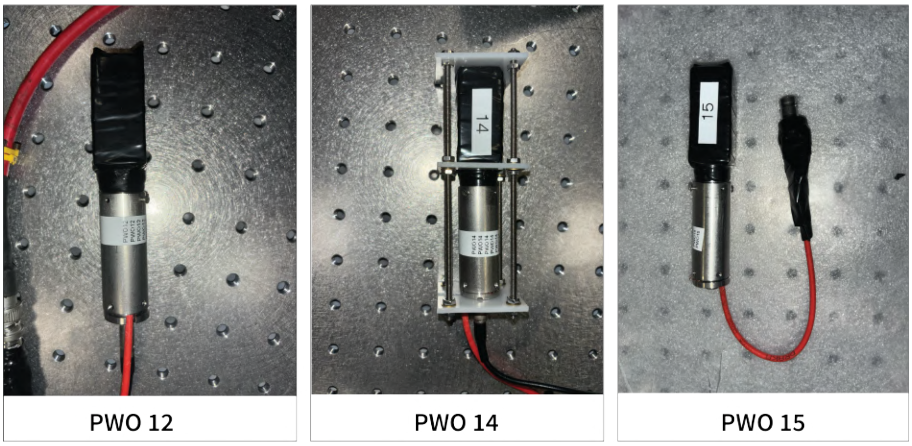

Figure 3.1: Functional PWO detectors, available at the GBAR Experiment.

In the section "Scintillator Characteristics", special considerations are outlined regarding the selection of the PWO4 scintillator for the study of positronium annihilation. The section "PMT Characteristics" describes some important features of the Hamamatsu photomultiplier and its relevance to our specific application, particularly in terms of gain. The section "Main Considerations for the Characterizations" details the parameters and key considerations that were monitored and recorded during the detector characterization process.

3.2 Scintillators Characteristics

In gamma spectroscopy, scintillators are crucial for converting gamma ray energy into visible or ultraviolet light, which is then detected by photodetectors. Sodium iodide doped with thallium (NaI(Tl)) is widely used due to its high efficiency in gamma ray conversion and good energy resolution. Bismuth germanate (BGO), with its high density and atomic number, is preferred for detecting high-energy gamma rays due to its ability to absorb high-energy photons. Additionally, **lead tungstate (PWO)** stands out for its excellent energy resolution and high density, making it particularly advantageous in positronium annihilation studies. This is due to its ability to handle high-energy events with high precision and resolution, which facilitates the acquisition of detailed data in complex experiments.

PWO (Lead Tungstate) scintillators, emit light in the blue to green region, specifically between 400 and 550 nm. The decay time of these scintillators ranges from 5 to 15 ns. While inorganic scintillators are generally relatively slow, PWO is an exception with a decay time of 5 to 15 ns. *This is an important asset for the positronium anihilation study, since the decay time is pretty lesser than the positronium anihilation time (142 ns).*

The time signal of a scintillator is given by the expression

$$N(t) = Ae^{-\frac{t}{\tau_f}} + Be^{-\frac{t}{\tau_s}} \tag{3.1}$$

Where:

- N(t) is the number of emitted photons at the time t.
- A and B are proportional factors.
- τ_f and τ_s, are the decay constants of the fast and slow components.

The average energy required to create a photon in scintillators is partially used for ionization processes within the material, and some photons are lost due to reabsorption. The quantum efficiency of scintillators, typically ranging between 10% and 30%, indicates the fraction of gamma-ray energy converted into visible or ultraviolet light. This efficiency is a critical factor in positronium annihilation measurements [CM12], [Ric81]. High quantum efficiency is essential for maximizing event detection, while low photon loss minimizes the loss of crucial information.

In addition to quantum efficiency, other important parameters include the energy resolution of the scintillator [Kno00], which affects the ability to distinguish between photons of different energies. In positronium annihilation studies, where annihilation events produce photons with specific energies, good energy resolution allows for precise separation of relevant signals from background noise.

Key Parameters in Scintillators for Positronium Annihilation Measurement

- **Quantum Efficiency**: Generally between 10% and 30%. Crucial for maximizing event detection by converting gamma-ray energy into visible or ultraviolet light.
- **Energy Resolution**: Affects the ability to distinguish between photons of different energies, allowing precise separation of relevant signals from background noise.
- **Rise Time**: A fast rise time ensures that high-energy events are recorded with minimal distortion, which is important for rapid processes such as positronium annihilation.
- **Transit Time**: A short transit time minimizes the delay between photon interaction and detector response, improving temporal accuracy.
- **Coupling Quality**: Efficient coupling between the scintillator and the photomultiplier ensures effective conversion of light into electrical signals, reducing signal loss.

3.3 PMT Characteristics

The **HAMAMATSU H13175U** photomultiplier is a widely used device in light detection applications due to its high efficiency and sensitivity. According to the manufacturer's datasheet, the key specifications of the photomultiplier are as follows:

- **Rise Time**: 0.57 ns at a gain of 1000 V.
- **Transit Time**: 2.7 ns at a gain of 1000 V.

These parameters are crucial for the setup and operation of the photomultiplier in detection experiments:

Rise Time

- **Definition**: Rise time is the interval it takes for the signal to rise from 10% to 90% of its maximum value.
- **Importance**: A rise time of 0.57 ns indicates that the photomultiplier has a rapid response to changes in light intensity, which is essential for measuring events that occur over very short timescales.

Transit Time

- **Definition**: Transit time is the time taken for a signal to travel from the start of the pulse to the moment it reaches its peak.
- **Importance**: A transit time of 2.7 ns shows that the photomultiplier can process light pulses with a temporal resolution of approximately 2.7 ns. This is critical for applications requiring high temporal precision in detection.

The choice of photomultiplier gain has a significant impact on system performance:

Gain of 1000 V

- **Advantages**: The maximum gain of 1000 V provides high signal amplification, allowing for better detection of weak events.
- **Disadvantages**: At maximum gain, the photomultiplier may generate a high number of events, which can saturate the system and lead to excessive data accumulation. Additionally, high gain can increase noise levels, complicating the discrimination between useful signals and background noise.

Feasibility of Maximum Gain

- **Problems**: In the reaction chamber, a gain of 1000 V may become unfeasible due to the high frequency and quantity of detected events, potentially leading to saturation issues and possible loss of temporal resolution in detection.
- **Solution**: *To address these issues, it may be necessary to adjust the photomultiplier gain to a lower value that balances adequate signal amplification with the system's ability to handle the event load.*

The information provided on the rise time and transit time of the HAMAMATSU H13175U photomultiplier is crucial for setting up the detection system and implementing the trigger. Adjusting the photomultiplier gain according to the expected event load and specific experiment characteristics is essential for obtaining accurate data and avoiding operational issues in the reaction chamber [MKS20].

3.4 Main Considerations for the Characterizations

For the preliminary characterization of the detectors, several important factors must be considered:

1. **Temperature:** The temperature in the laser room (where the characterizations and coincidence measurements were performed) may differ from the average temperature of the reaction chamber in the GBAR experiment. This temperature difference could affect the detector response.

2. **Distance from the Radiation Source:** The radiation source was placed at the same distance and solid angle from the detectors (3 cm). It was positioned close enough to maximize the solid angle but not so close as to increase the uncertainty in the distance.

3. **Trigger Level:** The trigger level must be appropriate. Unlike many commercial detectors, our detector does not have sphisticated built-in electronics. For adequate data acquisition, the trigger level should be high enough to avoid noise but not so high as to discard relevant data.

4. **Photomultiplier Gain:** This is a crucial parameter, as once the detectors are in place, they will be exposed to a large number of events. The gain level must be set appropriately to ensure that the detectors do not saturate and that all detectors have a consistent response.

5. **Time Windows:** When characterizing the detectors, it is necessary to use the same time window that covers the entire pulse duration for the calculation of the integral under the pulse.

In table **??** are shown some fenomenological and systamtic factors to consider during the characterization of the detectors, in order to ensure the traceability and the consistency for the subsequent calibration of the detectors.

Fenomenological Factors	**Systematic Factors**
Temperature	Trigger Level
Characteristics of the Radiative Source	Coupling of the Signal
Distance from Radiative Source	Time Window Analysis
Characteristics of the Detectors	Delay of the Signal
Detectors Gain	Integration Range
Compton Scattering	Noise Filtering

Table 3.1: Fenomenological and systematic factors to take into account for the characterization of the detectors.

3.5 Results of the Characterization

700 V Gain Level

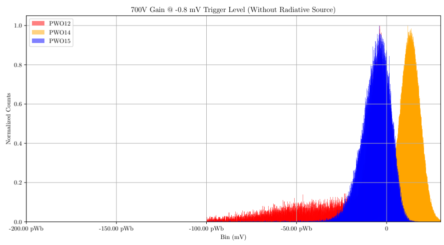

(a) Without Radiative Source

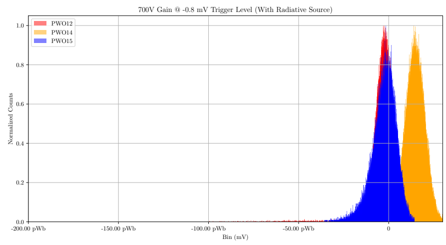

(b) With Radiative Source

Figure 3.2: ***700 V*** Gain level @ ***-0.8 mV*** Trigger Level, with and without radiative source.

800 V Gain Level

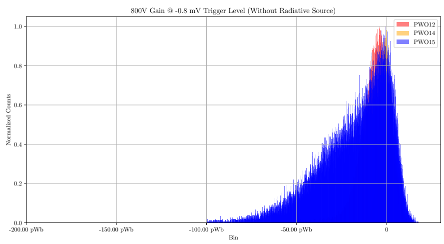

(a) Without Radiative Source

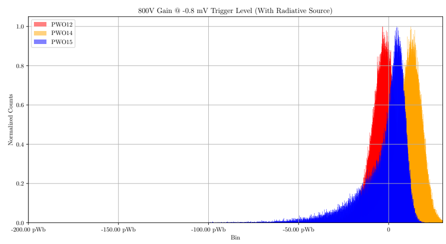

(b) With Radiative Source

Figure 3.3: ***800 V*** Gain level @ ***-0.8 mV*** Trigger Level, with and without radiative source.

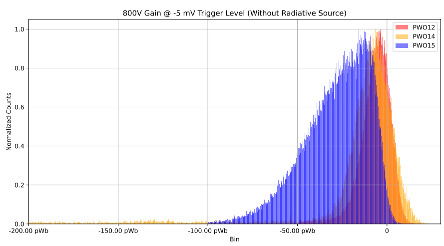

(a) Without Radiative Source

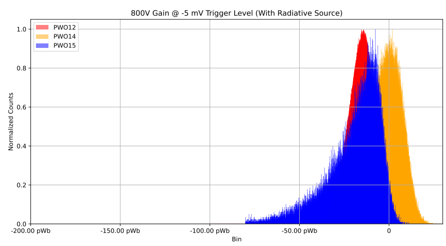

(b) With Radiative Source

Figure 3.4: ***800 V*** Gain level @ ***-5 mV*** Trigger Level, with and without radiative source.

900 V Gain Level

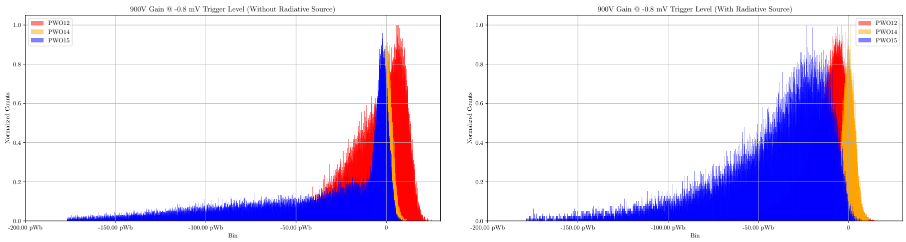

(a) Without Radiative Source (b) With Radiative Source

Figure 3.5: ***900 V*** Gain level @ ***-0.8 mV*** Trigger Level, with and without radiative source.

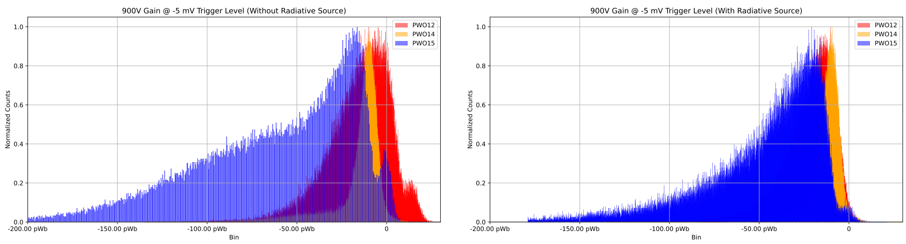

(a) Without Radiative Source (b) With Radiative Source

Figure 3.6: ***900 V*** Gain level @ ***-5 mV*** Trigger Level, with and without radiative source.

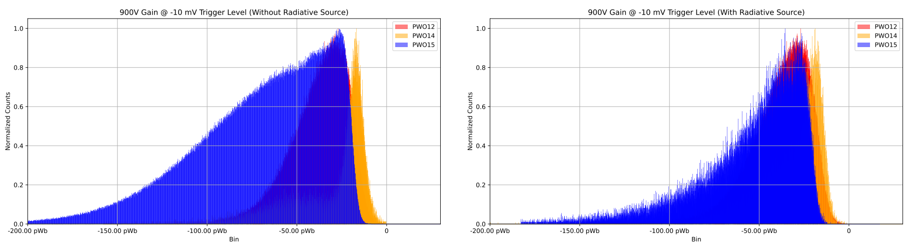

(a) Without Radiative Source (b) With Radiative Source

Figure 3.7: ***900 V*** Gain level @ ***-10 mV*** Trigger Level, with and without radiative source.

1000 V Gain Level

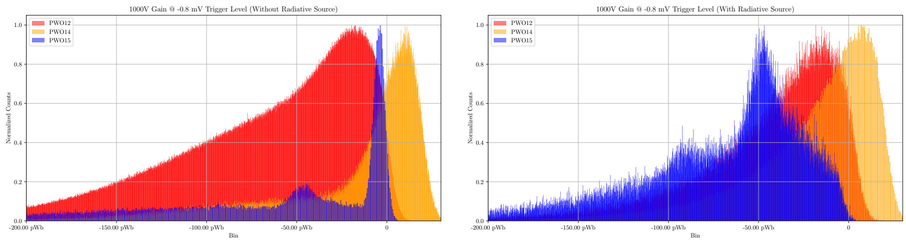

(a) Without Radiative Source (b) With Radiative Source

Figure 3.8: ***1000 V*** Gain level @ ***-0.8 mV*** Trigger Level, with and without radiative source.

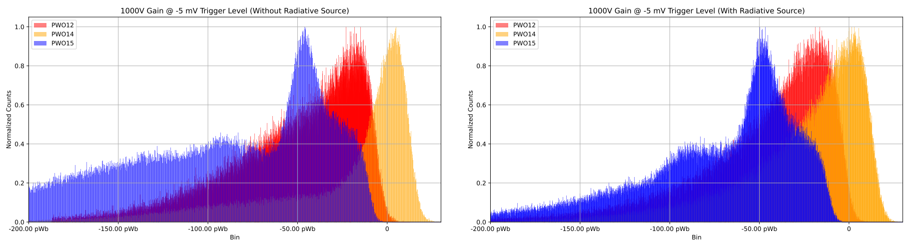

(a) Without Radiative Source (b) With Radiative Source

Figure 3.9: ***1000 V*** Gain level @ ***-5 mV*** Trigger Level, with and without radiative source.

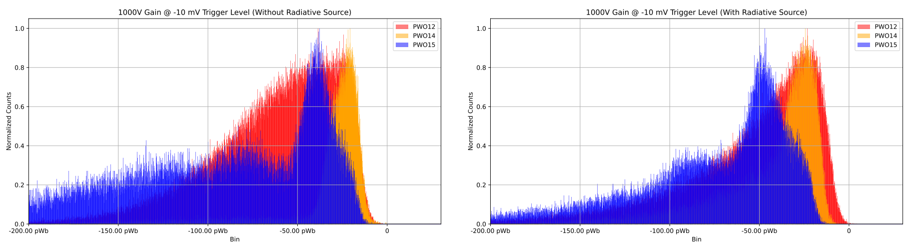

(a) Without Radiative Source (b) With Radiative Source

Figure 3.10: ***1000 V*** Gain level @ ***-10 mV*** Trigger Level, with and without radiative source.

Once the detectors have been implemented at the reaction chamber, a very important factor to consider is the magnetic field. It is a very well known fact, that the PMTs are quite sensible to magnetic fields variations. The work done by a 2024 summer student (Etienne Rosin) [Ros24] shows that there are significant variations of the magnetic fields, wihtin the GBAR area, upon a 13 consecutive days study.

3.6 Discussion of Results

The figure 3.2 shows the pulse integral distributions for the PWO 12, 14, and 15 detectors, with the photomultiplier gain set at 700 V. Due to the relatively low PMT gain, the event rate "approved" by the trigger, even at a low threshold of -0.8 mV, was too low to justify characterizing at higher trigger levels (at 700 V), as it would waste valuable work time.

First, it is observed (from figure 3.2) that the distributions for PWO 12 and PWO 15 are quite similar in both peak occurrence and their respective standard deviations. An interesting point is that PWO 12 exhibits a longer "tail" towards more negative values (down to -100 pWb) when no radiation source is present, compared to when a radiation source is introduced. Given that these graphs have been normalized by bin counts, one hypothesis is that this tail is linked to intrinsic pulses from the detector's electronics. Moreover, assuming that energy peaks are near zero, when the radiation source is added, the bins near zero dominate, effectively overshadowing the counts corresponding to more negative values associated with electronic effects.

The detector that stands out significantly at 700 V gain is PWO 14, with predominantly positive pulse integrals. At this gain level, counts in positive bins are noticeable, which is unexpected since we are working with negative pulses. However, it is important to mention that, as detailed in the next chapter, a specific time window had to be selected broad enough to capture positive areas where the signal exhibited overshoot. Nevertheless, if we assume that the overshoot behavior is fairly consistent, the overall "shape" of the distribution remains the same, only shifted towards positive values.

At 800 V gain (figures 3.3 & 3.4), the event detection rate on the oscilloscope was significantly higher, allowing us to perform tests with trigger levels of -0.8 mV and -5 mV. It's important to note that, during characterization, it was difficult to precisely interpret what we were observing whether a specific peak corresponded to an energy level, for instance. This is why conducting the characterization with different trigger levels allowed us to examine the distribution of more negative pulse levels. The test showed that adjusting the trigger level appeared to shift the peak positions, but in reality, it was simply cutting off the portion near zero. What seemed like a new peak was just the continuation of the truncated one.

An interesting observation at 800 V gain (see figure 3.3) is that, with a trigger level of -0.8 mV and no radiation source, the peaks of the pulse integral distributions for the detectors coincide, although all three exhibit very different standard deviations. However, when a radiation source is introduced, the peaks shift from their initial coincidence (without the source) to different positions further to the right, showing much more similar and reduced standard deviations. Once again, something particular happens with the PWO 14 detector: when the radiation source is introduced, the number of more positive bins with recorded counts increases for the established time window.

At 900 V gain (figures 3.5, 3.6 & 3.7), the first striking observation is the wide range of more negative bins characteristic of the PWO 15 detector, both with and without a radiation source. For this same detector (PWO 15), at the same trigger level, introducing a radiation source causes a peak to dominate at more negative bin values. This trend is generally observed in the other two detectors as well, and is, in fact, the expected behavior. This can be explained by the fact that at higher gains, assuming electronic effects remain consistent, the signal-to-noise ratio improves, revealing a noticeable difference in the detector characteristics with and without the radiation source.

An interesting observation regarding PWO 12 and PWO 15 at 900 V gain is that, in the absence of a radiation source, two significant peaks are present. However, when a radiation source is introduced, only one peak is visible. This behavior is not observed in the PWO 14 detector.

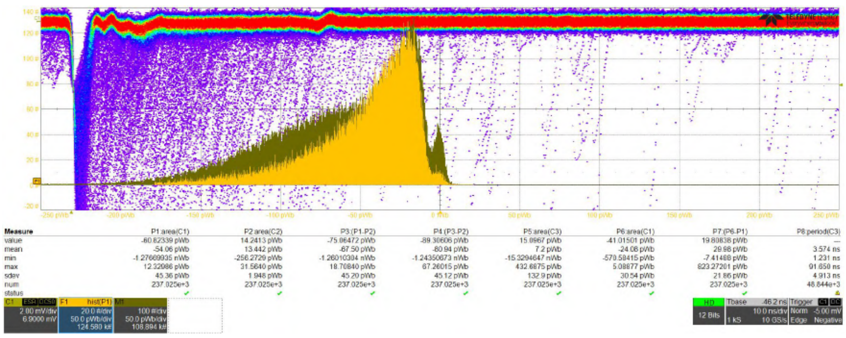

Figure 3.11: A characteristic time signal for the PWO15, at a 900 V gain level, is displayed using a persistance setup of 20 seconds.

The figure 3.11 shows a visualization of the oscilloscope screen while characterizing the PWO 15 detector at 900 V with a -5 mV trigger level and a persistence setting of 20 s. The persistence allows for observing consistent patterns of electronic effects, such as oscillations following the negative pulse and afterpulses occurring after the main pulse. At this point, it is not trivial to attribute the abnormal characteristics of PWO 15 to a consistent electronic effect or to an effective differentiation between the presence and absence of a radiation source, potentially due to an increased signal-to-noise ratio.

At a gain of 1000 V, there is practically no difference in the characteristics of the detectors with or without a radiation source. The only significant variation is observed in the PWO 15 detector, at this gain and with a -0.8 mV trigger level. In the absence of a radiation source, it shows a peak near zero, while in the presence of a radiation source, there is a noticeable absence of any peak near zero. The figure 3.12 illustrates an irregular yet consistent electronic effect in the PWO 15 detector at a gain of 1000 V. This effect consists of a series of irregular oscillations around the 0 V line.

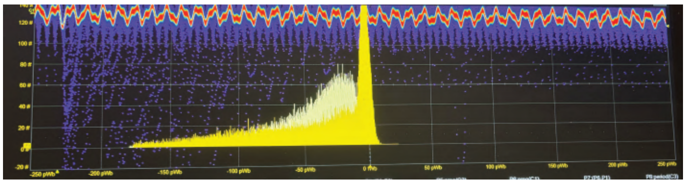

Figure 3.12: Irregular electronic effect observed in the PWO15 detector, for a 1000 V gain level

One of the key challenges during the characterization process was selecting the appropriate time window. While the main pulse consistently occurred within a certain time frame, many pulses were still developing beyond that window, leading to uncertain areas with no clear physical meaning. Even at the edges of the interval, where the dominant pulses were observed, afterpulses would appear, making the choice of the time window even more difficult.

However, assuming these "effects" are consistent—an assumption supported by the red-highlighted regions on the oscilloscope when using a 20-second persistence—phenomena like overshooting would generate positive areas. These consistent magnitudes would shift the characteristic curve to the right, reflecting a systematic behavior in the detected signal.

One attempt to mitigate these electronic effects was using a 2.5-bit filter. Unfortunately, the result was the same, as shown in figure 3.13, as the filter only smoothed the signal but didn't eliminate the overshoots responsible for the positive areas.

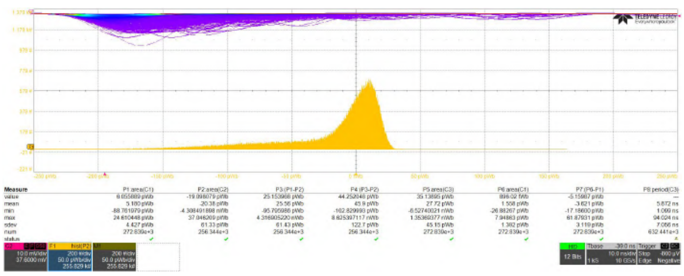

Figure 3.13: Application of a noise filter to the PWO14 time signal, and the correspondant distribution of the pulses, for a 1000 V gain, in presece of a radiative source.

During preliminary attempts to characterize the PWO 13, no significant signal was observed at any of the four gain levels (700 V, 800 V, 900 V, and 1000 V), whether in the presence or absence of radiation. This lack of response led us to a qualitative comparison with the other detectors. Given the absence of a signal, we decided to disassemble the detector (see figure 3.14), discovering poor optical coupling and irregularities on the crystal surface caused by residual optical glue. These irregularities could result in optical aberrations when photons hit the photocathode, potentially explaining the detector's lack of performance.

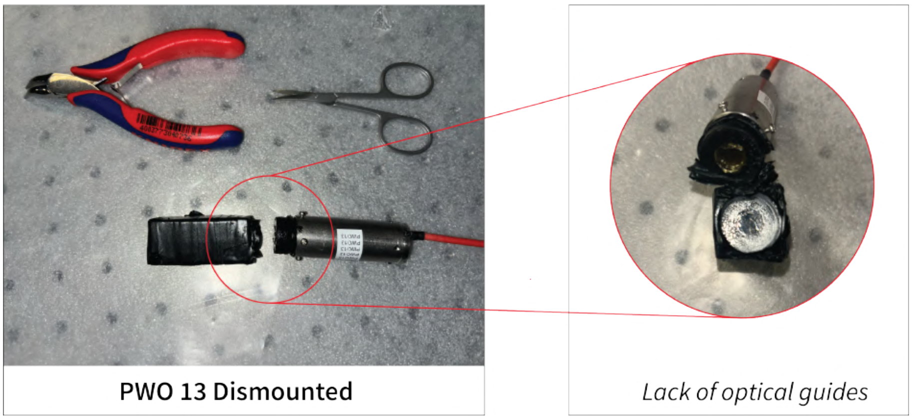

Figure 3.14: Dismounting of PWO13 allowed us to confirm the lack of optical guides, wich explains the irregular signal provided by this detector.

CHAPTER 4

Coincidence Measurement

4.1 Coincidence Detection and True Coincidence Rate in Experimental Setups

Introduction

In particle and nuclear physics experiments, accurately detecting and analyzing particle interactions often requires the use of multiple detectors, each positioned to capture different aspects of the interaction. A key technique in such experiments is *coincidence detection*, where signals from two or more detectors are observed simultaneously (or within a small time window) to confirm that they are related to the same physical event. This method significantly reduces the likelihood of false detections caused by random noise or unrelated events.

Coincidence Detection Concept

A *coincidence design* involves multiple detection channels (typically labeled as q), each capable of detecting signals from particle interactions. The goal is to ensure that signals detected by different channels can be correlated with each other based on time, space, or the properties of the interaction. When all q channels detect signals that are temporally and spatially correlated, a *coincidence event* is recorded. The level of coincidence—referred to as *q-fold coincidence*—depends on the number of channels involved. For example:

- **2-fold coincidence** requires simultaneous signals in 2 detectors.
- **3-fold coincidence** requires simultaneous signals in 3 detectors, and so on.

True Coincidence Rate Formula

The rate at which true correlated coincidence events occur in an experimental setup with q coincidence channels is given by:

$$R_q = q \cdot \tau^{q-1} \cdot \prod_{1}^{q} N_q$$

Where:

- R_q: The true coincidence rate, or the rate at which all q detectors detect correlated events.

- τ: The resolving time, or the time window within which the signals must be detected to be considered coincident. This is a critical parameter, as it controls the strictness of the coincidence requirement.

- N_q: The detection rate for each channel, representing the number of events per second that each detector registers.

Explanation of the Formula

- **Resolving Time (τ):** The resolving time τ is crucial in determining whether detected signals are genuinely correlated. A narrow resolving time (small τ) ensures that only closely timed signals are considered coincident, reducing the chance of accidental coincidences. However, as the number of channels q increases, the likelihood of all signals falling within this narrow window decreases, which is why τ is raised to the power of $q - 1$.

- **Detection Rate (N_q):** The detection rate N_q for each channel is the frequency at which each detector records signals. The product of these rates, $\prod_1^q N_q$, represents the overall likelihood that all q detectors are triggered during a single event. If any detector has a low detection rate, it decreases the overall probability of observing a coincidence.

- **Coincidence Multiplicity (q):** The multiplication by q accounts for the different possible sequences in which q detectors could be triggered by the same event.

In practice, this formula guides the design and adjustment of experimental setups to optimize the detection of true coincidence events. By carefully choosing the resolving time τ and ensuring that the detectors have sufficient sensitivity (i.e., adequate detection rates N_q), researchers can maximize the rate of true coincidences. This is particularly important in experiments where rare or complex particle interactions are studied, and distinguishing these from random noise or background events is crucial.

Determining the Pulse Integral Range in a $PbWO_4$ Detector for 0.511 MeV Gamma Photons

Summary

The objective of this experiment was to identify the range of pulse integrals in a $PbWO_4$ (lead tungstate) detector corresponding to the detection of 0.511 MeV gamma photons. A sodium-22 (^{22}Na) source, which emits both 1.21 MeV and 0.511 MeV gamma photons, was used for this purpose. A plastic scintillator served as a reference, while pulses were recorded in the $PbWO_4$ detector to analyze the correlation between the signals from both detectors.

Introduction

Sodium-22 is a radioactive isotope that decays by emitting a positron, which, upon annihilating with an electron, produces two 0.511 MeV gamma photons emitted in opposite directions. Additionally, the excited ^{22}Ne nucleus, resulting from the decay, emits a 1.21 MeV gamma photon. In this experiment, a plastic scintillator was used to detect the 1.21 MeV gamma photons, and the response of the $PbWO_4$ detector was simultaneously recorded to determine the range of pulse integrals corresponding to the 0.511 MeV photons.

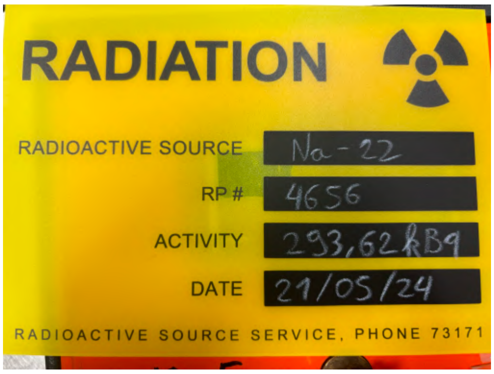

Figure 4.1: Sodium-22 radioactive isotope, with a 293,62 kBq activity, by may 21th of 2024..

Methodology

1. **Detector Configuration:**
    - The plastic scintillator was configured with an energy threshold to detect only 1.21 MeV gamma photons, acting as a trigger for the experiment.
    - The $PbWO_4$ detector was positioned so that when the plastic scintillator detected a 1.21 MeV photon, the $PbWO_4$ would be in a position to detect one of the 0.511 MeV photons resulting from positron-electron annihilation.
2. **Data Recording:**
    - Each time the plastic scintillator detected a 1.21 MeV photon, the corresponding pulse from the $PbWO_4$ was recorded.
    - The integral under each recorded pulse in the $PbWO_4$ was calculated, as it is proportional to the energy of the detected photon.
3. **Analysis:**
    - Sufficient coincidence data was collected to construct a histogram of the pulse integrals from the $PbWO_4$ detector.
    - A peak corresponding to 0.511 MeV photons was observed in the distribution of integrals.

4.2 Results

Distribution of Pulse Integrals for PS

To perform coincidence measurements, a reliable reference detector is essential in this case, a plastic scintillator, whose characteristics are well known. This detector must offer good resolution, high quantum efficiency, and, most importantly, an excellent signal-to-noise ratio. In the figure 4.2, you can see the energy characterization of the plastic scintillator (PS), showing two prominent peaks. The first peak, at higher energies (to the right), corresponds to 0.511 MeV photons, while the second peak, at lower energies (more negative), represents 1.21 MeV photons.

Based on this, a threshold level was set so the trigger (-91 mV) would only activate upon detecting 1.21 MeV photons. This step is crucial because, when connecting other detectors to separate channels, the PS will provide the trigger. Therefore, when the PS detects a 1.21 MeV gamma photon, the signal from the detector under test must either correspond to background noise or to a 0.511 MeV gamma photon. This setup ensures precise and controlled measurements.

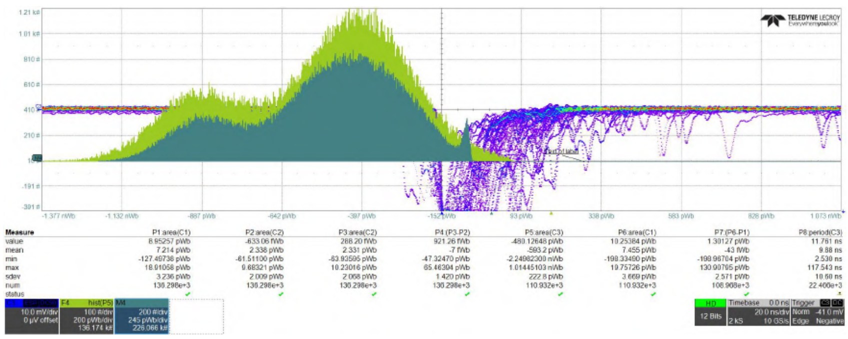

Figure 4.2: Identification of the correspondant voltage trigger level for the 1.2 MeV gammas, on the plastic scintillator.

Coincidence Measurement Attempt: Distribution of Pulse Integrals for PWO Detectors

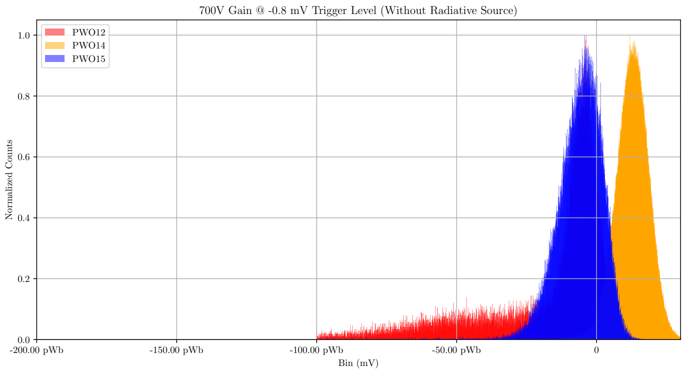

Figure 4.3: Integral distribution of the PWO detectors, for a 700 V gain, and a -0.8 mV trigger level, without source of radiation.

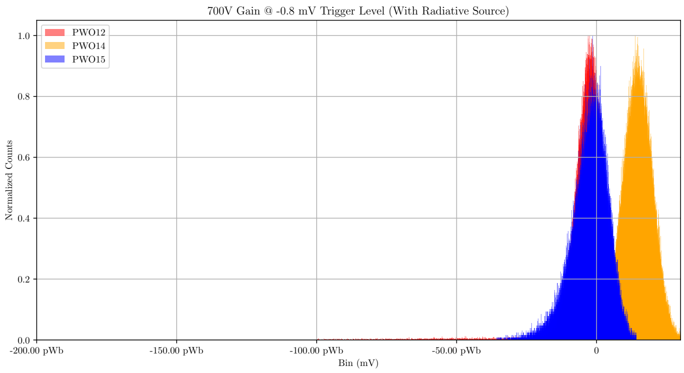

Figure 4.4: Integral distribution of the PWO detectors, for a 700 V gain, and a -0.8 mV trigger level, with source of radiation.

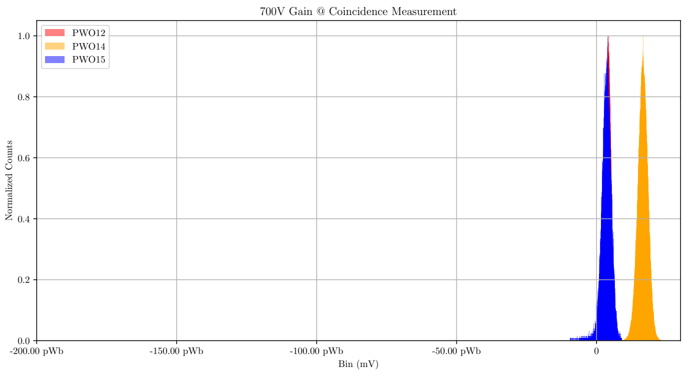

Figure 4.5: Coincidence measurement attempt, for a 700 V gain level

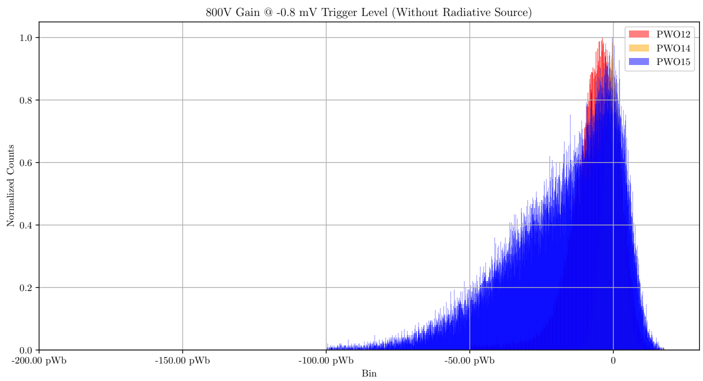

Figure 4.6: Integral distribution of the PWO detectors, for a 800 V gain, and a -0.8 mV trigger level, without source of radiation.

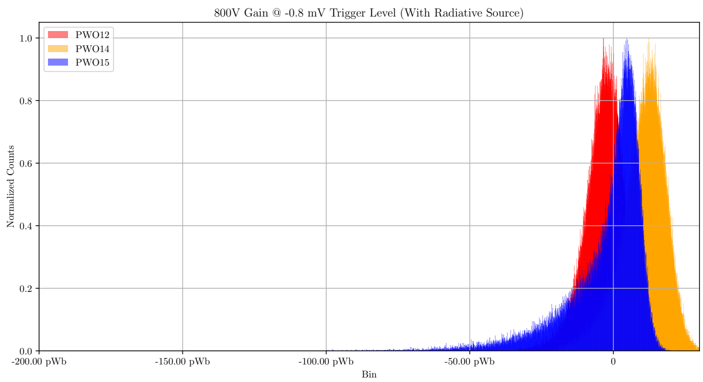

Figure 4.7: Integral distribution of the PWO detectors, for a 800 V gain, and a -0.8 mV trigger level, with source of radiation.

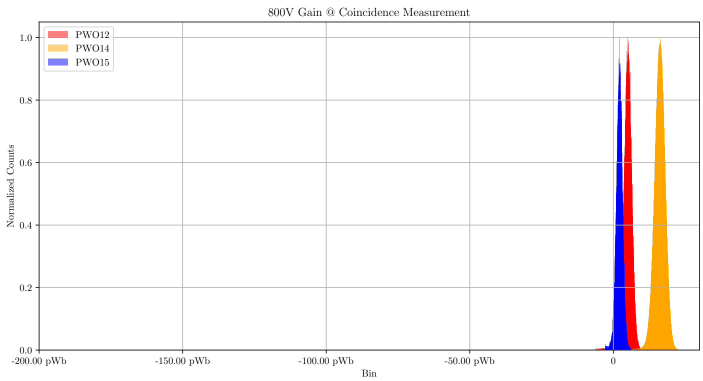

Figure 4.8: Coincidence measurement attempt, for a 800 V gain level

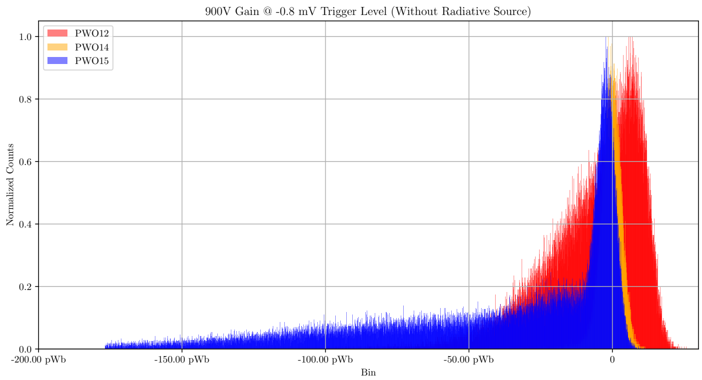

Figure 4.9: Integral distribution of the PWO detectors, for a 900 V gain, and a -0.8 mV trigger level, without source of radiation.

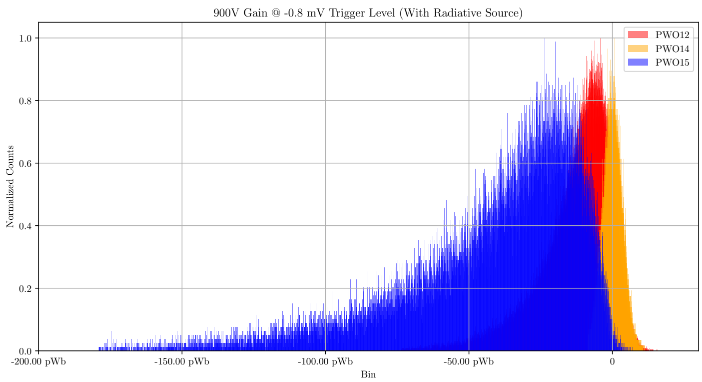

Figure 4.10: Integral distribution of the PWO detectors, for a 900 V gain, and a -0.8 mV trigger level, with source of radiation.

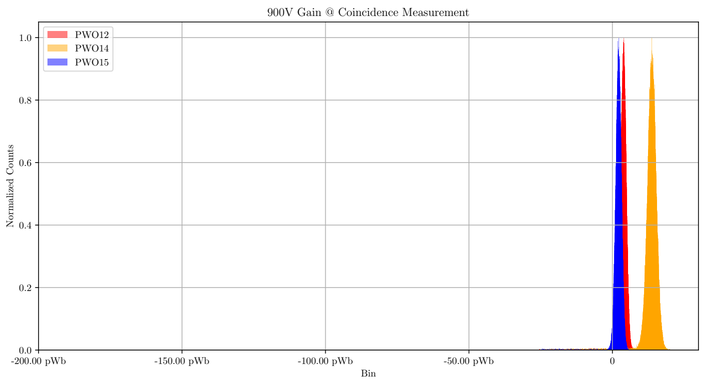

Figure 4.11: Coincidence measurement attempt, for a 900 V gain level

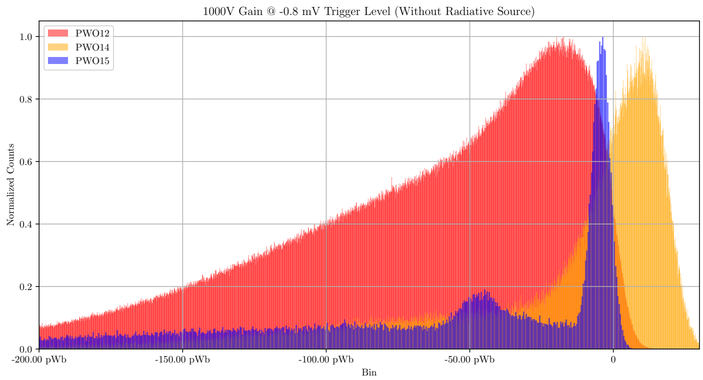

Figure 4.12: Integral distribution of the PWO detectors, for a 1000 V gain, and a -0.8 mV trigger level, without source of radiation.

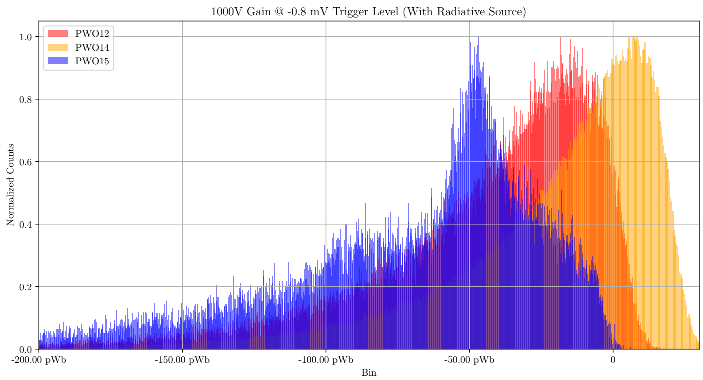

Figure 4.13: Integral distribution of the PWO detectors, for a 1000 V gain, and a -0.8 mV trigger level, with source of radiation.

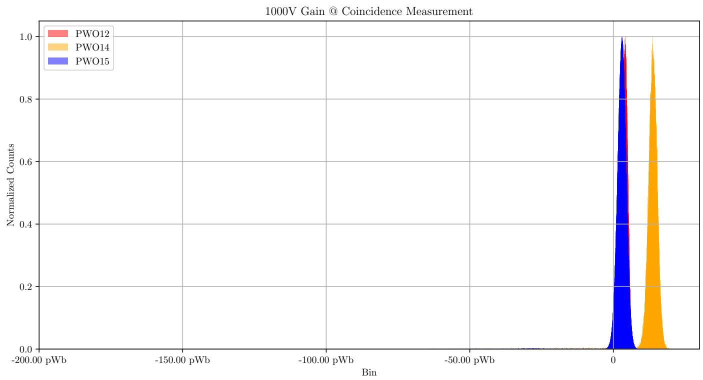

Figure 4.14: Coincidence measurement attempt, for a 1000 V gain level

Coincidence Measurement Attempt: Distribution of Pulse Integrals for PWO Detectors

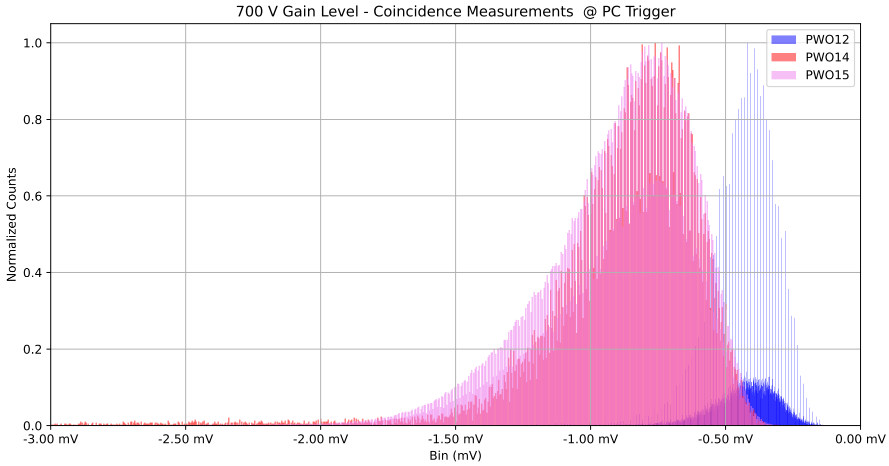

Figure 4.15: Coincidence measurement for a ***700 V*** gain level. Distribution of voltage levels is shown.

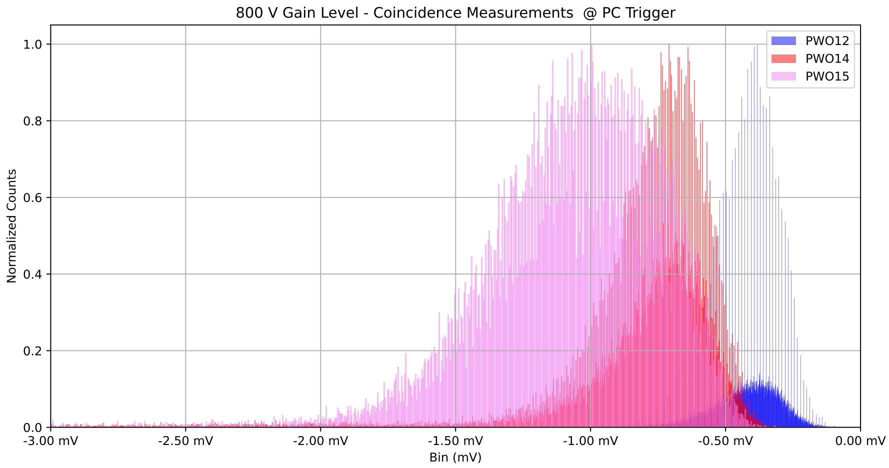

Figure 4.16: Coincidence measurement for a ***800 V*** gain level. Distribution of voltage levels is shown.

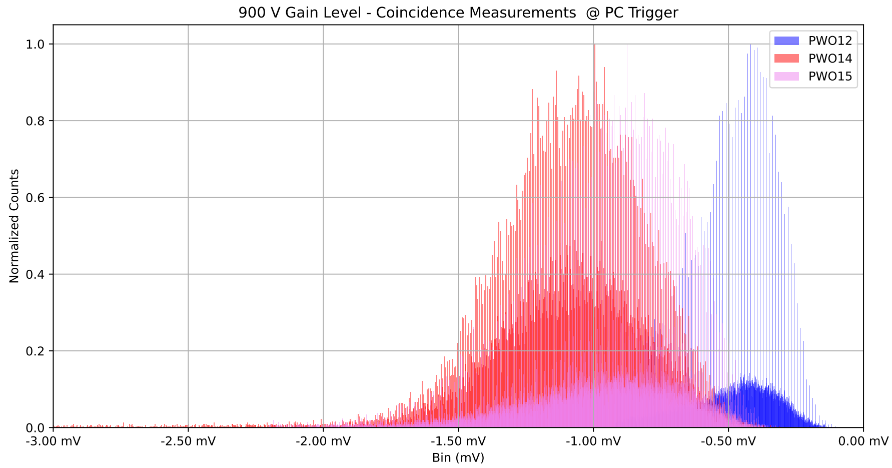

Figure 4.17: Coincidence measurement for a ***900 V*** gain level. Distribution of voltage levels is shown.

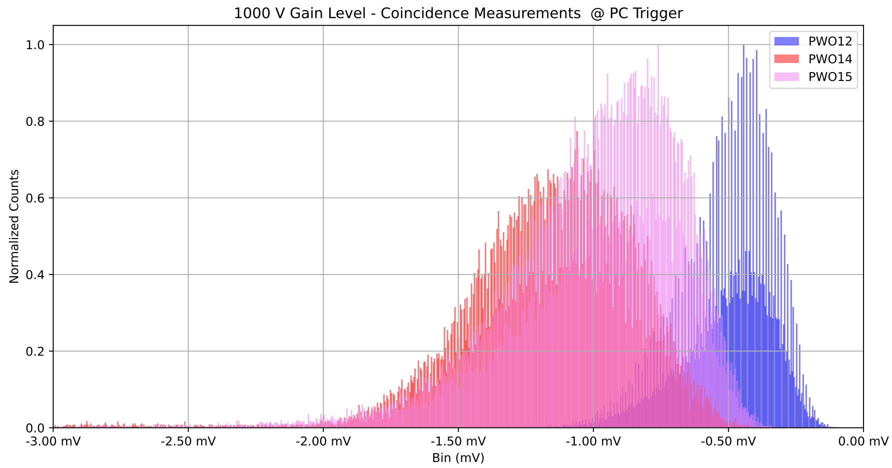

Figure 4.18: Coincidence measurement for a ***10 00 V*** gain level. Distribution of voltage levels is shown.

4.3 Discussion

In general terms, conducting a coincidence measurement based on the distribution of pulse integrals proved challenging. Electronic effects such as overshooting and afterpulses persisted, even when using the plastic scintillator as the trigger. These effects resulted in positive areas with no physical meaning. Another notable issue was the low number of events observed using the Na-22 radiation source.

Due to the lack of suitable electronic equipment for signal processing and difficulty in logistics to establish a reliable comparison pattern (e.g., at a linac facility where positron annihilation is well-known), a constant time base of 10 ns/div was chosen for all trials. This includes both the characterizations from the previous chapter and the coincidence measurements undertaken here.

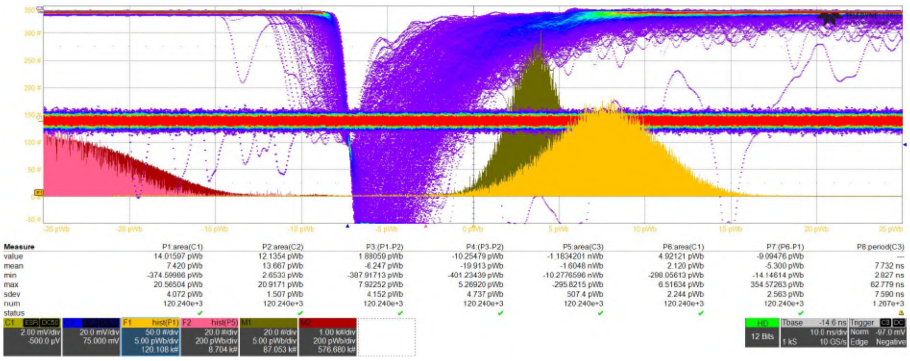

Figure 4.19: A 10 ns/div timebase provides a broad enough time window to visualize PS pulses and PWO pulses in coincidence.

The rationale for using a fixed 10 ns/div time base lies in the assumption that electronic effects are relatively constant and consistent across different gain levels. As a result, there should be a correspondence between the individual characteristics of the detectors and the range obtained in the pulse distributions during the coincidence measurement.

The 10 ns/div time base was selected because it provided a sufficient time window for coincidence measurements, which are time-critical. The window needed to account for the longer pulse duration of the plastic scintillator, which exceeds that of the primary pulses from the PWO detectors, as well as the occurrence window of the PWO pulses. In fact, before any formal characterizations or measurements were made, a preliminary trial was conducted to determine the required time window (10 ns/div), which was then applied consistently to both the characterizations in the previous chapter and the coincidence measurements described here.

Once the coincidence measurement for the pulse integral distributions was completed, a new coincidence measurement was undertaken to analyze the lower voltage levels (i.e., pulse voltages) for different gain settings on each PWO detector, as shown in the figures 4.15 to 4.18. The shape of these distributions is quite interesting, revealing a series of evenly spaced peaks that form two crests within the same distribution. As the gain level increases, the voltage range in coincidence expands, and more negative peak values are observed.

It would be valuable to replicate this distribution for the detectors both with and without a radiation source, using different trigger levels. This would help identify which parts of each detector's characteristic distribution correspond to the patterns observed in the figures 4.15 to 4.18.

CHAPTER 5

Practical Results

5.1 Methodology

Once the detectors are fully characterized, they are intended to be used for identifying positronium annihilation within the GBAR reaction chamber. The GBAR reaction chamber is equipped with a movable target, allowing for the exchange between a silicon target and a mesoporous silicon target, the latter being the positron-positronium conversion material. In essence, when the target is mesoporous silicon and a positron beam is injected, positronium formation occurs.

Positronium annihilation within the reaction chamber has been confirmed, which presents a challenge when calculating the cross-section for Hbar (antihydrogen) formation from positronium and antiprotons (pbar). Since some of the positronium annihilates, there is uncertainty about how much of the initially formed positronium actually reacted with the antiprotons, complicating the measurements.

If the amount of annihilated positronium is known, it becomes possible to conduct a more accurate measurement of the cross-section. But how can the annihilated positronium be measured? First, the silica target will serve as a control—meaning no positronium formation—while the mesoporous silicon target will lead to positronium formation. PWO detectors are placed in the well of the reaction chamber. It is important to note that in both cases, with and without positronium, positron annihilation events occur, releasing two gamma photons of 0.511 MeV in opposite directions.

These gamma photons will strike the PWO crystals, causing the release of visible light photons. These photons then hit the photocathode of the PMT (photomultiplier tube), liberating a primary electron, which is accelerated across several dynodes to produce a voltage output from the PMT. The signal is captured by an oscilloscope and subsequently analyzed.

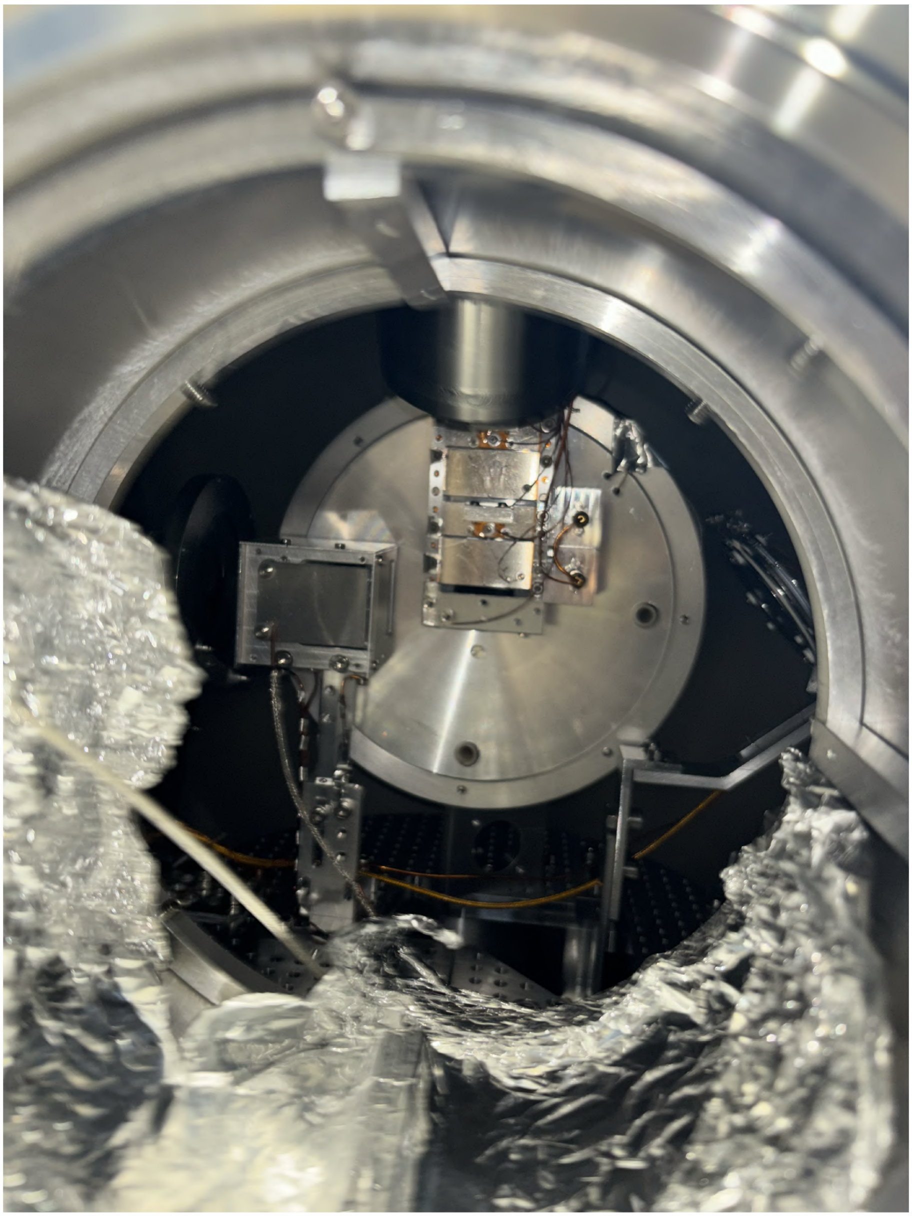

Figure 5.1: Reaction chamber open. At the image it is possible to visualize the Silica and Mesoporous Silica Targets.

The methodology involved taking multiple shots with the detectors in both conditions: without positronium (silicon target) and with positronium (mesoporous silicon target). Additionally, the tests were repeated for each control case, but this time with tungsten blocks placed in front of the detectors. The purpose of placing these tungsten blocks was to block the gamma photons directly originating from the target—those directly associated with annihilation events. This way, the only gamma photons reaching the detectors would be those linked to Compton scattering, which is significant given the high number of events and the high-density material of the reaction chamber.

By isolating the Compton-scattered gammas, this setup aimed to filter out direct annihilation signals, providing a clearer understanding of the secondary gamma interactions within the chamber.

Stage	**Actions/Conditions**	**Objective**
Target Preparation	Silicon Target (*control*, without positronium). Mesoporous Silicon Target (with positronium).	Establish conditions for the formation or absence of positronium.
Detector Placement	Place PWO detectors in the reaction chamber.	Detect positron annihilation events.
Experiments Without Positronium	Use the silicon target as a reference (*control*).	Compare signals with positronium experiments.
Experiments With Positronium	Use the mesoporous silicon target to facilitate positronium formation.	Detect and measure the positronium produced.
Use of Tungsten Blocks	Experiments without tungsten blocks (detectors capture direct gammas). Experiments with tungsten blocks (block direct gammas).	Identify gammas scattered by the Compton effect.
Signal Measurement	Capture signals from detectors using an oscilloscope. Repeat experiments in both conditions (with and without positronium).	Record differences in detected events.
Results Analysis	Compare captured signals under different conditions (positronium vs *control*, with and without tungsten blocks).	Determine the amount of annihilated positronium.

Table 5.1: Summary of the methodology used for the detection and analysis of positronium in the reaction chamber of the GBAR experiment.

5.2 Analysis of the PWO Detectors Signals

The figure 5.2 displays the averages of the signals corresponding to shots conducted with mesoporous silica, which facilitates the formation of positronium. Two conditions are shown: without the tungsten block and with the tungsten block. It is important to note that the vertical scale is normalized and presented in logarithmic scale, allowing for a more detailed observation of the detected signals.

There are two key details worth highlighting when observing these signals. The first is that the peak signal is higher in the case without the tungsten block compared to the case with the tungsten block. This is consistent with the fact that by blocking the gammas that directly originate from the target where positronium is generated, the amount of energy deposited in the scintillator is reduced, resulting in lower signal values.

The second is that once the decay time has elapsed, a certain parallelism in the shape of the signals can be observed, indicating similar rates of change, despite the differing peak magnitudes. This is particularly noteworthy given that the peak values of both signals are significantly different from each other, while the decay rates remain quite similar for both cases.

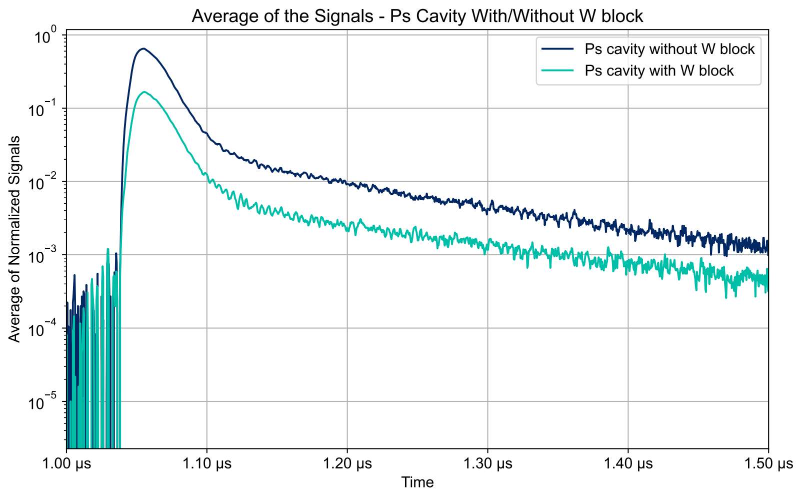

Figure 5.2: Comparison of the average of the signals, for the Ps cavities, with and without the W block

The figure 5.3 presents a comparison of the average signals in the absence of a tungsten block, specifically for the silicon cavities and the positronium (Ps) cavities. At first glance, it is evident that the peak values of the average signals for both cases are nearly identical. However, the peak value of the positronium signal is slightly lower, which can be attributed to the fraction of positrons that do not annihilate and instead are deposited in the mesoporous silica to form positronium.

Once the decay time elapses, no parallel tails are observed, unlike what was seen in the previously illustrated case. Instead, it is noted that the tail is longer in the case of the positronium (Ps) cavity, where a higher decay time is observed compared to the silicon case. This difference corresponds to the positronium that has annihilated in the mesoporous silica target. Within the GBAR experiment, trials have been conducted, and a method has been established to correlate the annihilated positronium from these time signals.

From a broader perspective, these findings resonate with ongoing research within the GBAR experiment, where understanding positronium dynamics is essential for calculating the cross-section of antihydrogen production from positronium and antiprotons. The ability to correlate annihilated positronium with time signals not only enhances our understanding of particle interactions but also opens up new avenues for precision measurements in fundamental physics.

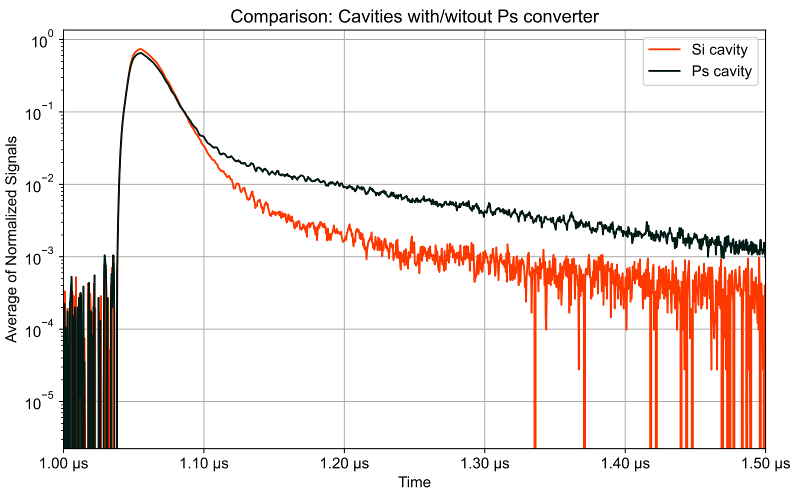

Figure 5.3: Comparison of the average of the signals, *for the Ps and Si cavities.*

The figure 5.4 displays the average signals for the four experimental scenarios: with and without positrons, and with and without the tungsten block. This comprehensive view reveals important insights into the effects of the tungsten shielding on signal behavior. Notably, the peak signal values from the scintillators when shielded by the tungsten block were consistently lower than those observed without the block. This observation aligns well with the expectation that the tungsten effectively attenuates the gamma radiation emitted from the targets.

Interestingly, even in both conditions—whether with or without the tungsten block—the peak signal associated with positronium was slightly lower than that observed in its absence. This suggests that the presence of positronium introduces additional factors affecting signal intensity. Moreover, the positronium signal exhibited a longer decay tail compared to the signals in the absence of positronium. This behavior could be indicative of the unique characteristics of positronium interactions within the mesoporous silica, reflecting the complexities of energy deposition and annihilation processes.

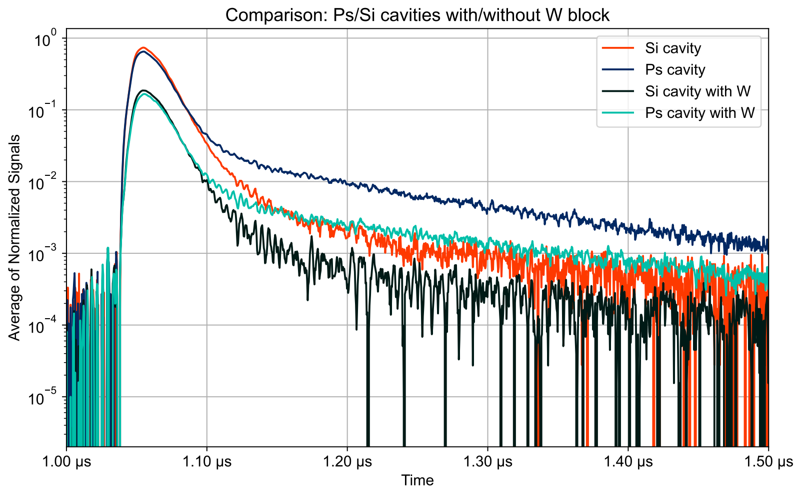

Figure 5.4: Comparison of the average of the signals, *for the Ps and the Si cavities*, with and without the **W block**.

The figures 5.5 and 5.6, display the signals corresponding to ortho-positronium and silicon, both with the tungsten block in place. By applying a fit to the data, a time constant of 155 ns was observed. Given that the known lifetime of ortho-positronium is approximately 142 ns, this result confirms that the tail of the signal carries important information related to the annihilation process of positronium. The slightly longer times observed, compared to the expected lifetime of ortho-positronium, could likely be attributed to Compton scattering events. These scattering interactions would cause a delay in the signal decay, as gamma photons scatter within the experimental setup, thereby extending the observed time constants. This reinforces the idea that the tungsten block effectively blocks direct gamma rays but still allows for secondary Compton-scattered events to contribute to the signal, adding complexity to the analysis of positronium annihilation.

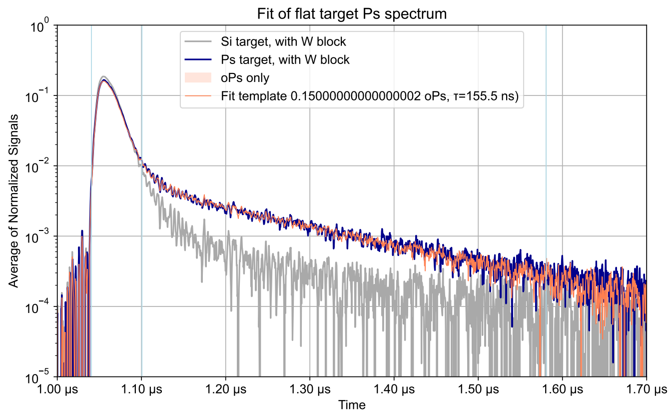

Figure 5.5: Fit of flat target Ps Spectrum.

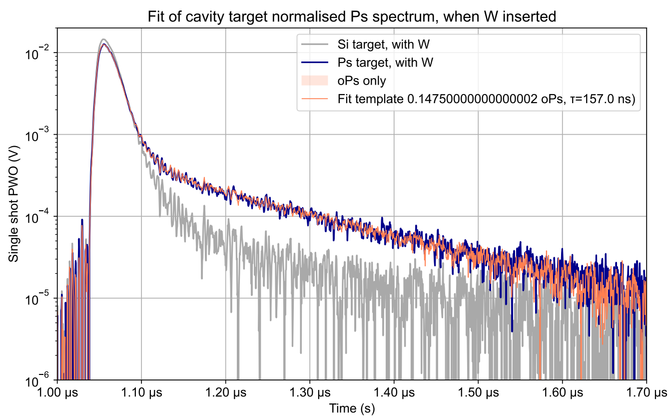

Figure 5.6: Fit of cavity target normalised Ps spectrum, when W inserted.

5.3 Results of the GEANT4 Simulations

Karol Szymczyk, a PhD student currently engaged in the GBAR experiment, has made significant strides with his Geant4 simulation, which accurately models the intricate geometry of the reaction chamber, including the targets made of silica and mesoporous silica. The simulation is particularly notable because it explores two critical scenarios: one without the tungsten block and one with it. These conditions allow for a thorough examination of energy deposition, specifically highlighting the nuances in how gamma rays interact with the detector materials.

The preliminary results (see figures 5.7 & 5.8) reveal crucial insights, especially regarding the identification of 0.511 MeV gamma rays, which are signatures of positron and positronium annihilation. The ability to distinguish these gammas across both setups offers a strong validation of the simulation's effectiveness in replicating real-world conditions within the reaction chamber. The tungsten block's role in absorbing or scattering gamma rays that would otherwise directly impact the PWO detectors is an especially important finding. This suggests that the block efficiently shields the detectors from direct annihilation events, allowing for a more focused study of scattered photons, including those from Compton scattering, which was also identified in the simulation.

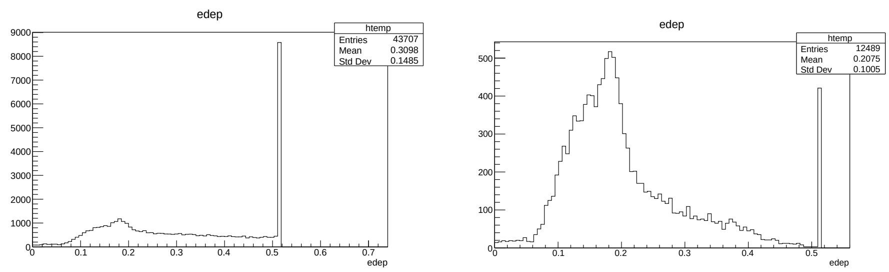

(a) Without Led Tungsten Block (b) With Led Tungsten Block

Figure 5.7: Simulation results of the energy deposition within the PWO detector for a positronium target, both without and with a tungsten lead block.

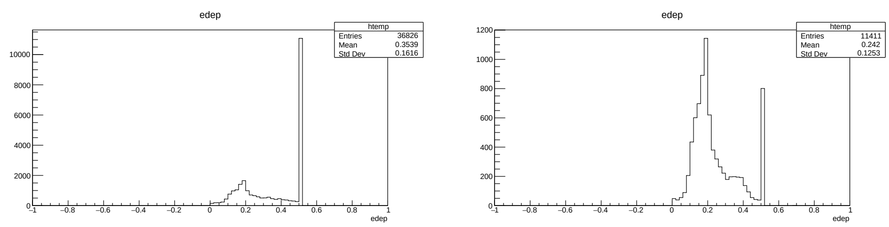

(a) Without Led Tungsten Block (b) With Led Tungsten Block

Figure 5.8: Simulation results of the energy deposition within the PWO detector for a silica target, both without and with a tungsten lead block.

The juxtaposition of the two configurations—without the tungsten block, where direct annihilation gammas dominate, and with the block, where scattered events become more pronounced—provides a valuable framework for understanding how these energy depositions differ in real-time experiments. Szymczyk's work, by simulating this controlled environment, helps to infer the broader impact of secondary gamma interactions and allows for optimization of the detector setup for future experiments.

Furthermore, the identification of positronium annihilation through gamma ray detection serves as a key metric for evaluating the performance of the reaction chamber. The fact that the simulation can reliably differentiate between positron and positronium annihilation means that future detector developments can be better calibrated for precision, leading to more accurate measurements of positronium behavior under experimental conditions. This is especially crucial for GBAR, where precise knowledge of positronium annihilation is essential for measuring cross sections and advancing the understanding of antihydrogen formation.

Conclusion

The study of positronium annihilation within the GBAR experiment's reaction chamber, supported by lead tungstate (PWO) detectors, has unveiled both significant progress and key technical challenges. While the detectors successfully captured annihilation events, unwanted electronic effects, such as overshooting and oscillations,compromised the clarity of signals, especially at higher gain levels. These effects highlight the intricate nature of the experimental setup and emphasize the need for more advanced techniques to mitigate them. With expanded access to the lab, a more refined characterization could be conducted, focusing on the distribution of minimum pulse values. Additionally, implementing specialized compensators or filters to minimize these effects would greatly enhance the quality of the captured data.

It would also be invaluable to conduct these characterizations in a reference environment, such as the linac output, where positron annihilation is well understood. This would allow for more precise comparisons with the results obtained inside the reaction chamber, ensuring the reliability of the measurements. Another key factor, the suppression of Compton scattering, remains critical; addressing this issue with appropriate techniques would significantly improve the precision of the detected events.

All in all, this meticulous work lays a solid foundation for future experiments in positronium annihilation detection, unlocking new avenues for exploration. Despite the challenges faced, the results affirm the significance of this project, showing that the technical hurdles encountered are an opportunity for further advancement in the characterization of fundamental particle interactions. With the refinements and improvements mentioned, the potential for future discoveries is vast, positioning this work as a crucial step toward a deeper understanding of subatomic particles and their behaviors.

Bibliography

[BP80] Berko, S. and Pendleton, H. N. “Positronium Chemistry”. In: *Annual Review of Nuclear and Particle Science* vol. 30, no. 1 (1980), pp. 543–581.

[CM12] Cassidy, D. B. and Mills, A. P. “Experimental Progress in Positronium Laser Physics”. In: *Physics Today* vol. 65, no. 8 (2012), pp. 38–43.

[Kan+21] Kanai, Y. et al. “Precision Spectroscopy of Positronium: Testing Bound-State QED Theory”. In: *Journal of Physics B: Atomic, Molecular and Optical Physics* vol. 54, no. 1 (2021), p. 015001.

[Kno00] Knoll, G. F. *Radiation Detection and Measurement*. 3rd. John Wiley & Sons, 2000.

[Mil48] Milne, E. A. “Positronium”. In: *Nature* vol. 162, no. 4124 (1948), pp. 487–488.

[MKS20] Moskaleva, V., Kalikhov, A., and Shevchenko, M. “Gamma-ray Spectroscopy in High-energy Physics Experiments”. In: *Journal of Physics: Conference Series* vol. 1400, no. 1 (2020), p. 012048.

[Ric81] Rich, A. “Recent Experimental Work on Positronium in Gases”. In: *Reviews of Modern Physics* vol. 53, no. 1 (1981), pp. 127–165.

[Ros24] Rosin, E. A. *MagGiver: Mapping of the GBAR Magnetic Field*. Submitted by etienne.alex.rosin@cern.ch. CERN. Geneva. EP Department, July 2024.